

ExoMol line lists – XXXVIII. High-temperature molecular line list of silicon dioxide (SiO₂)

A. Owens,^{1*} E.K. Conway,^{1,2} J. Tennyson^{1†} and S. N. Yurchenko^{1‡}

¹ Department of Physics and Astronomy, University College London, Gower Street, WC1E 6BT London, UK

² Atomic and Molecular Physics Division, Center for Astrophysics | Harvard & Smithsonian, Cambridge, Massachusetts 02138, USA

Accepted XXXX. Received XXXX; in original form XXXX

ABSTRACT

Silicon dioxide (SiO₂) is expected to occur in the atmospheres of hot rocky super-Earth exoplanets but a lack of spectroscopic data is hampering its possible detection. Here, we present the first, comprehensive molecular line list for SiO₂. The line list, named OYT3, covers the wavenumber range 0–6000 cm⁻¹ (wavelengths $\lambda > 1.67 \mu\text{m}$) and is suitable for temperatures up to $T = 3000$ K. Almost 33 billion transitions involving 5.69 million rotation-vibration states with rotational excitation up to $J = 255$ have been computed using robust first-principles methodologies. The OYT3 line list is available from the ExoMol database at www.exomol.com.

Key words: molecular data – opacity – planets and satellites: atmospheres – stars: atmospheres – ISM: molecules.

1 INTRODUCTION

In the gas phase, silicon dioxide (²⁸Si¹⁶O₂) is a linear triatomic molecule, analogous to CO₂. SiO₂ is expected to be present in the atmospheres of hot rocky super-Earth exoplanets (Tennyson & Yurchenko 2017a). These tidally-locked exoplanets are in close proximity to their host star with their dayside exposed to temperatures reaching 4000 K. At such high temperatures the material on the surface of the planet vaporises to produce an atmosphere strongly dependent on initial planetary composition (Schaefer & Fegley 2009; Miguel et al. 2011), e.g. composed of SiO₂-rich silicates like the Earth’s continental crust (Schaefer et al. 2012). Furthermore, the likely presence of water vapour creates a steam atmosphere, and since all major rock-forming elements (Si, Mg, Ca, etc.) dissolve in steam to some extent, one can expect to encounter simple molecules composed of rock-forming elements with oxygen and hydrogen (Fegley et al. 2016).

Investigating the spectroscopy of hot rocky super-Earths requires accurate molecular opacities on systems such as SiO₂. There is, however, very limited information on some of these molecules, partly because they form in the gas phase at very high temperatures making their spectra challenging to measure in the laboratory. Instead, theory offers a more viable route for generating the molecular line lists of these systems through systematic approaches based on first-principles methodologies (Tennyson 2016; Tennyson & Yurchenko 2017b). These computational procedures have been successfully adopted by the ExoMol database (Tennyson & Yurchenko 2012; Tennyson et al. 2016), which provides comprehensive line lists suitable for modelling exoplanet atmospheres at elevated temperatures. Already a large number of important diatomic and polyatomic species have been treated within the ExoMol framework (Tennyson & Yurchenko 2018), and efforts are now being focused on molecules relevant to hot rocky super-Earth atmospheres. This brings about its own unique set of challenges, notably the completeness of the line list at very high temperatures and the lack of experimental data to refine the theoretical spectroscopic model.

Regarding SiO₂, only a few studies have investigated its infrared spectrum with measurements of the ν_2 bending mode (Andrews & McCluskey 1992) and ν_3 stretching mode (Schnöckel 1978; Schnöckel 1980). However, since these studies were performed in solid argon matrices the measured wavenumbers can be shifted by tens of wavenumbers (Jacox 1994) making it difficult to assess the usefulness of the determined values for gas phase studies. Similarly, only a small number of theoretical

* The corresponding author: alec.owens.13@ucl.ac.uk

† The corresponding author: j.tennyson@ucl.ac.uk

‡ The corresponding author: s.yurchenko@ucl.ac.uk

studies have considered silicon dioxide (Kaufman et al. 1967; Pacansky & Hermann 1978; Wang et al. 1996; Brinkmann et al. 1999; Kostko et al. 2009; Hao et al. 2014), but none of these are particularly relevant to the work presented here, namely the high-accuracy calculation of its rotation-vibration spectrum.

In this work, we present the first, comprehensive rotation-vibration line list of gas-phase SiO₂. The new line list has been computed using robust first-principles methodologies (Tennyson 2016) within the ExoMol computational framework (Tennyson & Yurchenko 2017b) and adds to the other available silicon-bearing molecules in the ExoMol database: SiH₄ (Owens et al. 2017), SiH (Gorman et al. 2019), SiO (Barton et al. 2013), SiS (Upadhyay et al. 2018) and SiH₂ (Clark et al. 2020).

2 METHODS

The computational approach used to produce the SiO₂ line list is described in detail in the supplementary material and only a brief summary is provided here. Initially, high-level *ab initio* methods were used to compute the potential energy surface (PES) and dipole moment surface (DMS) of the electronic ground state of SiO₂. The PES was generated using explicitly correlated coupled cluster (CCSD(T)-F12b) calculations with extrapolation to the complete basis set limit, and included several additive energy corrections to account for small effects like scalar relativity. This approach is capable of producing accurate PESs for closed-shell molecules that can reproduce fundamental term values to within ± 1 cm⁻¹ on average (e.g. see Owens et al. (2018) and references within). Due to the lack of reliable experimental data for this molecule, the PES was not empirically refined. The DMS was computed using CCSD(T)-F12b with a large augmented correlation consistent basis set. It is now well established that transition intensities computed using *ab initio* DMSs are comparable to, and occasionally more reliable, than experiment (Yurchenko 2014; Tennyson 2014). Both surfaces were computed on the same grid of 15 365 nuclear geometries and then fitted with suitable analytic representations for use in the next stage of the calculation process. The potential energy and dipole moment surfaces are provided as supplementary material along with Fortran routines to construct them.

Line list calculations employed the variational nuclear motion program TROVE (Yurchenko et al. 2007), which was extended to treat linear triatomic molecules in this work. Benchmarking was performed against the triatomic nuclear motion code DVR3D (Tennyson et al. 2004) to ensure the validity of the TROVE implementation. The ability to utilise two nuclear motion codes based on different methodologies proved highly beneficial and meant the theoretical spectroscopic model of SiO₂ could be checked for consistency. This was particularly important given the lack of experimental data to compare against. A large symmetry-adapted basis set was used in the rovibrational calculations with convergence testing performed at different J values.

The line list was computed with a lower state energy threshold of $hc \cdot 15\,000$ cm⁻¹ (h is the Planck constant and c is the speed of light) and considered transitions up to $J = 255$ in the 0–6000 cm⁻¹ range. The energy levels and wavefunctions of SiO₂ can be classified under the $C_{2v}(\text{M})$ molecular symmetry group (Bunker & Jensen 1998). The nuclear spin statistical weights are $g_{\text{ns}} = \{1, 1, 0, 0\}$ for states of symmetry $\{A_1, A_2, B_1, B_2\}$, respectively. Thus, B_1 and B_2 states need not be computed and transitions follow the symmetry selection rules $A_1 \leftrightarrow A_2$; and the standard rotational selection rules, $J' - J'' = 0, \pm 1$, $J' + J'' \neq 0$; where $'$ and $''$ denote the upper and lower state, respectively. These representations are correlated to the $D_{\infty h}(\text{M})$ irreducible representation, commonly used for linear molecules, as $A_1 \leftrightarrow \Sigma_g^+$ and $A_2 \leftrightarrow \Sigma_g^-$. Another standard spectroscopic descriptor is the Kronig parity e/f (Brown et al. 1975), related to the total parity $+1$ (A_1) and -1 (A_2) as follows: the parity of the e state is $(-1)^J$ while the parity of the f state is $(-1)^{J+1}$.

The vibrational quantum numbers used by TROVE (see supplementary material) were correlated to the following standard spectroscopic quantum numbers used for linear-type triatomic molecules: $v_1, v_2^{\text{lin}}, L = |l|, v_3$, where v_1 and v_3 are the symmetric and asymmetric stretching quantum numbers, respectively, v_2 is the bending vibrational quantum number used for linear molecules and l is the corresponding vibrational quantum number. The two bending quantum numbers v_2^{lin} and l are connected to the ‘non-linear’ bending quantum number v_2 by $v_2^{\text{lin}} = 2v_2 + l$ with $L = v_2^{\text{lin}}, v_2^{\text{lin}} - 2, \dots, 0(1)$.

The symmetries of the vibrational and rotational contributions span the A_1, A_2, B_1 and B_2 irreducible representations (irreps) in $C_{2v}(\text{M})$ and $\Sigma_{g/u}^{+/-}$ ($L = 0$), $\Pi_{g/u}$ ($L = 1$), $\Delta_{g/u}$ ($L = 2$) etc. in $D_{\infty h}$. Odd values of the quantum number v_3 indicates vibrational states of B_2 symmetry. The rotational quantum number k_a is constrained to the vibrational angular momentum by $k_a = l$.

A total of 32 951 275 437 transitions involving 5 688 942 energy levels up to $J = 255$ were computed for the OYT3 line list. The distribution of lines and levels as a function of J is illustrated in Fig. 1. The largest number of transitions in the OYT3 line list occurs between $J = 39 \leftrightarrow 40$, while the number of states peaks at $J = 46$ before smoothly decreasing, a result of the upper state energy threshold of $hc \cdot 21\,000$ cm⁻¹.

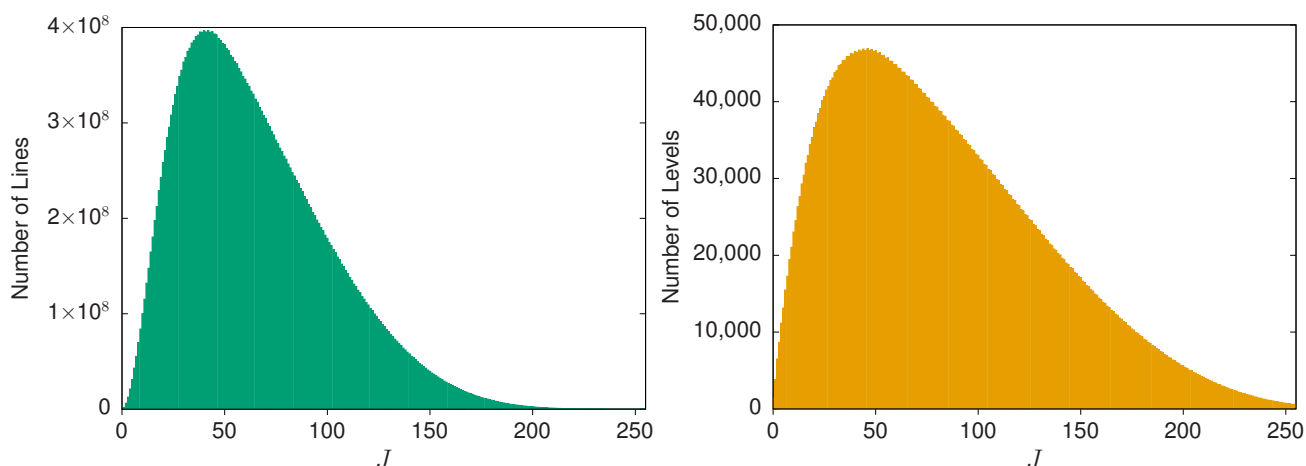


Figure 1. The total number of lines (left panel) and energy levels (right panel) for each value of the rotational quantum number J in the OYT3 line list. For the number of lines, a single J value counts transitions between $J \leftrightarrow J-1$ and $J \leftrightarrow J$.

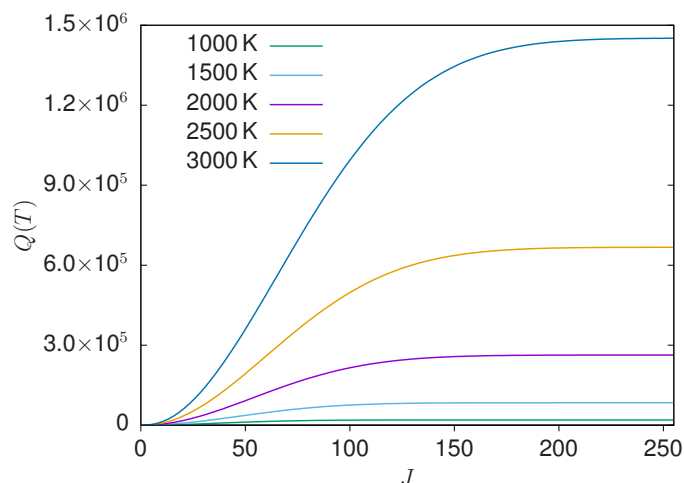


Figure 2. Convergence of the partition function $Q(T)$ of SiO₂ with respect to the rotational quantum number J at different temperatures.

3 RESULTS

3.1 Partition function of silicon dioxide

The temperature-dependent partition function $Q(T)$ is expressed as,

$$Q(T) = \sum_i g_i \exp\left(\frac{-E_i}{kT}\right), \quad (1)$$

where $g_i = g_{\text{ns}}(2J_i + 1)$ is the degeneracy of a state i with energy E_i and rotational quantum number J_i . Values of the partition function of SiO₂ have been computed by summing over all calculated rovibrational energy levels on a 1 K grid in the 1–3000 K range (provided as supplementary material). In Fig. 2, the convergence of $Q(T)$ as a function of J for select temperatures is shown. At lower temperatures the partition function converges quickly but a substantial number of high J states must be considered to achieve convergence above 1500 K. At $J = 255$, the value of $Q(2000 \text{ K})$ is converged to 0.0001%, while the value of $Q(3000 \text{ K})$ is converged to 0.0019%.

The SiO₂ line list was computed with a lower state energy threshold of $hc \cdot 15\,000 \text{ cm}^{-1}$. A measure of the completeness of the line list can be obtained by studying the reduced partition function $Q_{\text{red}}(T)$, which only includes energy levels up to $hc \cdot 15\,000 \text{ cm}^{-1}$ in the summation of Eq. (1). The ratio $Q_{\text{red}}(T)/Q(T)$ has been plotted with respect to temperature in Fig. 3 and from this we see that above 1500 K the ratio starts to decrease from unity. At 3000 K, the ratio $Q_{\text{red}}/Q = 0.90$ and this should be considered as a soft temperature limit for the OYT3 line list. Uses above this will result in a progressive loss of opacity but the missing opacity contribution can be estimated from Q_{red}/Q if needed (Neale et al. 1996).

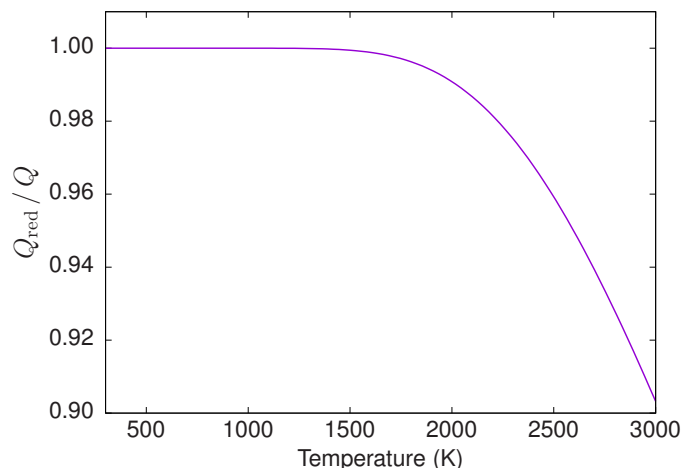


Figure 3. The ratio Q_{red}/Q as a function of temperature T ; this provides a measure of the completeness of the OYT3 line list.

Table 1. Extract from the `.states` file of the SiO₂ OYT3 line list.

i	\tilde{E}	g_{tot}	J	unc	Γ_{tot}	e/f	v_1	v_2^{lin}	L	v_3	C_i	n_1	n_2	n_3	Γ_{vib}	K	Γ_{rot}
1	0.000000	1	0	0.0	A1	e	0	0	0	0	1.00	0	0	0	A1	0	A1
2	578.229349	1	0	2	A1	e	0	2	0	0	1.00	0	0	1	A1	0	A1
3	990.856966	1	0	2	A1	e	1	0	0	0	1.00	1	0	0	A1	0	A1
4	1154.529779	1	0	4	A1	e	0	4	0	0	1.00	0	0	2	A1	0	A1
5	1570.947837	1	0	4	A1	e	1	2	0	0	1.00	1	0	1	A1	0	A1
6	1728.958462	1	0	6	A1	e	0	6	0	0	1.00	0	0	3	A1	0	A1
7	1977.509720	1	0	4	A1	e	2	0	0	0	1.00	1	1	0	A1	0	A1
8	2148.937437	1	0	6	A1	e	1	4	0	0	1.00	1	0	2	A1	0	A1
9	2301.592712	1	0	8	A1	e	0	8	0	0	1.00	0	0	4	A1	0	A1
10	2559.419897	1	0	6	A1	e	2	2	0	0	1.00	1	1	1	A1	0	A1

i : State counting number;

\tilde{E} : Term value (in cm^{-1});

g_{tot} : Total state degeneracy;

J : Total angular momentum quantum number;

unc: Estimated uncertainty of energy level (in cm^{-1});

Γ_{tot} : Overall symmetry in $C_{2v}(\text{M})$ (A_1 or A_2);

e/f : The Kronig (rotationless) parity;

$v_1, v_2^{\text{lin}}, L, v_3$: Linear-molecule vibrational quantum numbers;

C_i : Largest coefficient used in the TROVE assignment;

$n_1 - n_3$: TROVE vibrational quantum numbers;

Γ_{vib} : Symmetry of the vibrational contribution in $C_{2v}(\text{M})$;

K : Rotational quantum number, projection of J onto molecule-fixed z axis ($K = L$);

Γ_{rot} : Symmetry of the rotational contribution in $C_{2v}(\text{M})$.

3.2 Line list format

The SiO₂ line list is provided in the ExoMol data format and further details with illustrative examples can be found in Tennyson et al. (2016). The `.states` file, see Table 1, contains all the computed rovibrational energy levels (in cm^{-1}), each labelled with a unique state ID counting number, symmetry and quantum number labelling, and the contribution C_i from the largest eigencefficient used to assign the rovibrational state. The `.trans` files have been split into 100 cm^{-1} frequency bins for user-handling purposes and contain all computed transitions with upper and lower state ID labels and Einstein A coefficients, see Table 2.

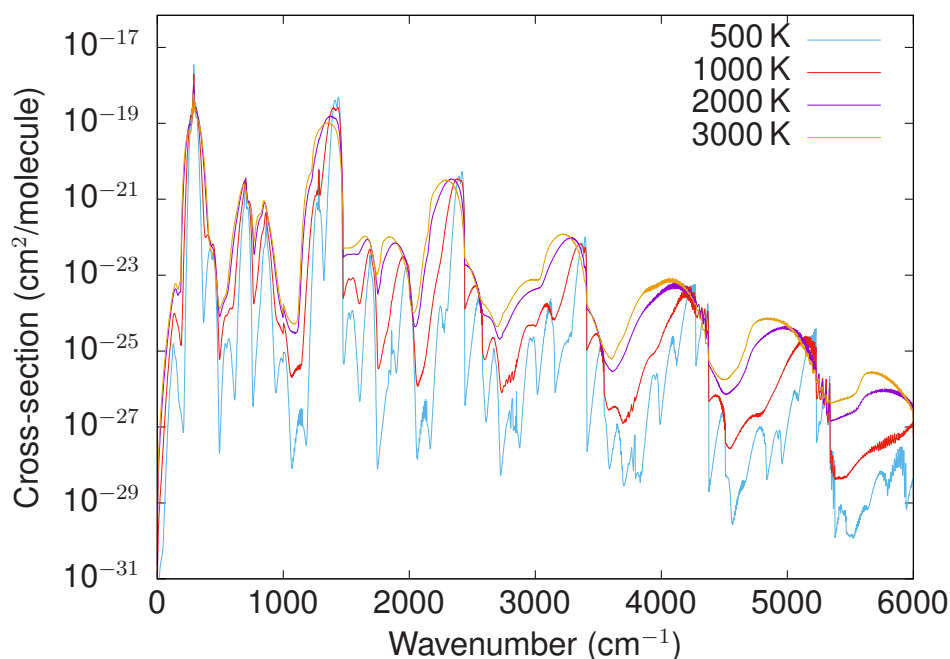
The assignment of the vibrational quantum numbers to each state is performed in TROVE by analysing the contribution from the primitive basis functions of the different modes, which are then converted to the linear-molecule, normal mode quantum numbers (see Table 1). The connection between the assignment and the primitive basis functions is not always straightforward due to the complicated contraction scheme used to build the final symmetrized rovibrational basis set (Yurchenko et al. 2017). Thus, in instances where the eigen-coefficient $|C_i|$ is very small the assignment should be considered as indicative.

The computed energy levels in the OYT3 line list have been assigned uncertainties (in cm^{-1}) in the following way: The three fundamental term values have been given an estimated uncertainty of 2 cm^{-1} , which has then been propagated to all

Table 2. Extract from the .trans file for the 0–100 cm⁻¹ window of the SiO₂ OYT3 line list.

f	i	A_{if}
1901572	1832882	8.4692e-44
2283835	2261046	9.7538e-45
948596	1016760	9.4147e-35
1830303	1853859	2.7761e-42
4120223	4135284	1.1104e-41
649389	670531	1.0237e-43
284492	332334	2.6832e-31
3288298	3306461	1.3021e-31
3796784	3812806	2.0901e-39
366209	348742	3.7795e-33

f : Upper state ID; i : Lower state ID;
 A_{if} : Einstein A coefficient (in s⁻¹).

**Figure 4.** Temperature dependence of the spectrum of SiO₂, which becomes increasingly flat as the temperature increases. Absorption cross-sections were computed from the OYT3 line list and represented with a Gaussian line profile with a half width at half maximum (HWHM) of 1 cm⁻¹ at a resolution of 1 cm⁻¹.

overtone and combination bands using the TROVE normal mode quantum numbers. For example, a state with ($n_1 = 5$, $n_2 = 2$, $n_3 = 1$) has an estimated uncertainty of 16 cm⁻¹. The initial uncertainty estimate of 2 cm⁻¹ for the fundamentals is based on our previous experience using similar levels of *ab initio* theory to construct closed-shell molecule potential energy surfaces (Owens et al. 2015a,b, 2016, 2018; Owens & Yurchenko 2019). This uncertainty scheme is approximate and should not be relied on in instances where the eigen-coefficient $|C_i|$ is small. We have also opted to round the estimated uncertainties to integer values so that they can be easily differentiated from more robust uncertainties, e.g. derived from experiment. Note that the ground state $J > 0$ rovibrational term values, i.e. ($n_1 = 0$, $n_2 = 0$, $n_3 = 0$) have been assigned uncertainties of 2 cm⁻¹ throughout.

3.3 Simulated spectra of silicon dioxide

The temperature dependence of the OYT3 line list is illustrated in Fig. 4, where we have plotted integrated absorption cross-sections at a resolution of 1 cm⁻¹ using a Gaussian profile with a half width at half maximum (HWHM) of 1 cm⁻¹. Spectral simulations were performed with the EXOCROSS program (Yurchenko et al. 2018). As expected, the SiO₂ spectrum becomes smoother and more featureless as the temperature increases. This is caused by the increased population of vibrationally excited states with temperature, leading to substantial broadening of the rotational band envelopes.

Stick spectra of the two strongest bands at a temperature of 1000 K are shown in Fig. 5, with the fundamental ν_2

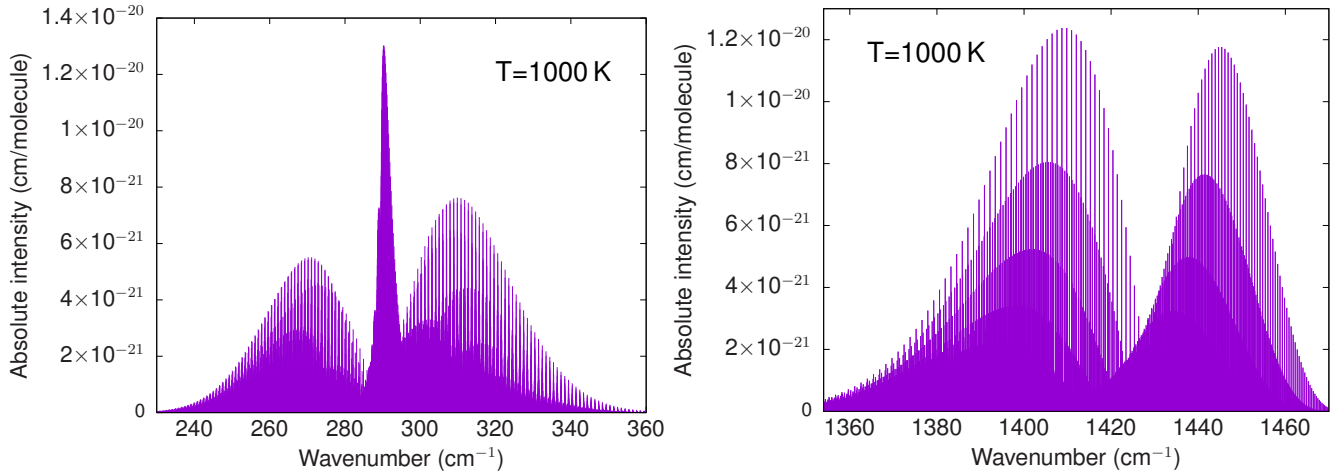


Figure 5. Stick spectrum of the two strongest bands of SiO₂ at $T = 1000$ K. The left panel shows the bending ν_2 (0,1,1,0) fundamental band while the right panel shows the stretching ν_3 (0,0,0,1) band, where states are labelled by the quantum numbers (v_1, v_2, L, v_3).

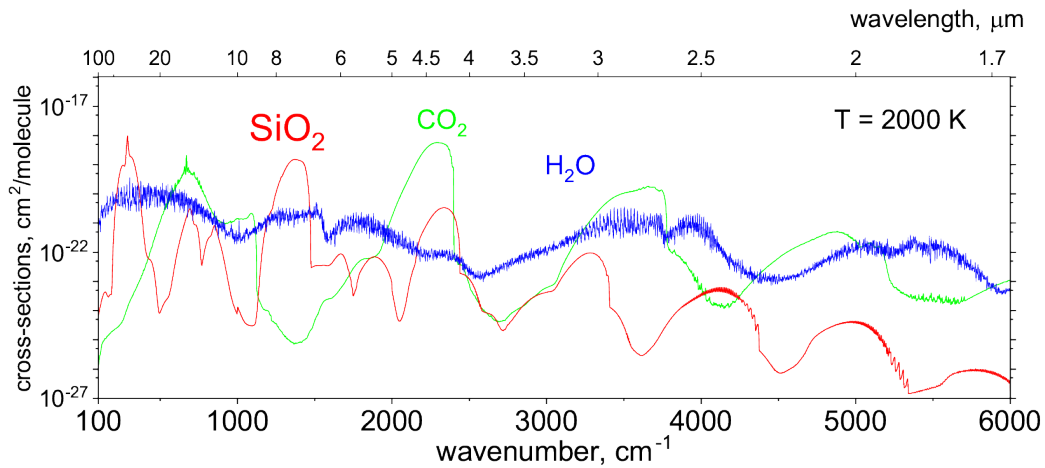


Figure 6. Comparison of the 2000 K broadband spectra of SiO₂, CO₂ and H₂O. A Gaussian line profile with HWHM of 1 cm^{-1} at a resolution of 1 cm^{-1} was used. The CO₂ cross sections were computed using the new UCL-4000 line list (Yurchenko et al. 2020) and the Pokazatel line list for H₂O (Polyansky et al. 2018). For clarity the relatively flat water spectrum has been reduced by a factor of ten. SiO₂ shows strong absorption features around 250 and 1500 cm^{-1} . A weaker SiO₂ feature at about 2300 cm^{-1} is masked by strong CO₂ absorption in this region.

bending mode (left-hand panel) and the stretching ν_3 band (right-hand panel) displayed. The position of these bands is in broad agreement with previous experimental studies (Andrews & McCluskey 1992; Schnöckel 1978; Schnöckel 1980) but given these infrared measurements were performed in solid argon matrices, which are known to shift the measured wavenumbers, we avoid a direct comparison.

The SiO₂ spectrum has a distinct strong feature at $4.5 \mu\text{m}$. This region plays an important role in the atmospheric applications of exoplanets due to the CO₂ photometric band used by the Spitzer Space Telescope (IRAC instrument). For example, this band was used to build the phase curve of super-Earth 55 Cancri e by Demory et al. (2016) and to provide analysis of the atmospheric (day/night) structure of the plane. The atmosphere was shown to have a high temperature contrast, from 1400 K (night side) to 2700 K (day side). In Fig. 6, we show that the CO₂ $4.5 \mu\text{m}$ region has strong overlap with the spectrum of SiO₂, namely the $(1, 4^0, 0)$ band in the same region, although the strongest absorption bands are $(0, 1^1, 0)$ and $(0, 2^2, 0)$ where states are labelled by the quantum numbers (v_1, v_2^L, v_3). An absorption spectrum of water is also shown for comparison. Silicon dioxide has also been suggested as a potential constituent of the atmosphere of the super-Earth Corot-7b (Schaefer et al. 2012) and thus should be included in retrievals for hot super-Earths.

4 CONCLUSION

A comprehensive molecular line list for SiO₂ has been presented. The line list, named OYT3, covers the 0–6000 cm⁻¹ range (wavelengths $\lambda > 1.67 \mu\text{m}$) for states below $J = 255$ and is applicable for temperatures up to 3000 K. As discussed above, the lack of reliable experimental spectroscopic data on SiO₂ has meant that the OYT3 line list has been constructed using purely *ab initio* methods with no degree of empirical refinement. The accuracy of the predicted line positions will suffer as a result, particularly for highly excited states and shorter wavelengths, but for the fundamental bands, which have the strongest intensity, the errors should be within 1–3 cm⁻¹ as a conservative estimate. The computed line intensities should not be overly affected and are largely expected to be within the 5–10% of experimentally determined intensities. Of course, without reliable experimental data to compare against these are only estimates based on our previous experience constructing *ab initio* spectroscopic models with similar electronic structure methods (see, for example, our work on SiH₄ (Owens et al. 2015b)).

The usual ExoMol methodology is to take advantage of laboratory measurements to improve the accuracy of our computed line lists (Tennyson 2012). However, in the absence of high-resolution spectroscopic measurements for SiO₂, this has not proved possible. In practice a number of current line lists are entirely *ab initio*. Of course, for few electron systems such as HD⁺ (Amaral et al. 2019), HD (Amaral et al. 2019), HeH⁺ (Engel et al. 2005; Amaral et al. 2019), H₃⁺ (Mizus et al. 2017) and LiH (Coppola et al. 2011) it is possible to compute high accuracy line lists which should reproduce astronomical spectra within their observational accuracy. The Molecular Opacity Database Project at the University of Georgia (UGAMOP) treated a number of many electron diatomics in this fashion, see Weck et al. (2003) for example. However, more pertinent here is the case of HCN. The original HCN / HNC line list of Harris et al. (2002) was based on a purely *ab initio* potential energy and dipole surfaces (van Mourik et al. 2001) computed at a lower level of theory, and hence of lower accuracy, than that employed here. This line list has been successively updated (Harris et al. 2006; Barber et al. 2014), and even adapted to H¹³CN (Harris et al. 2008), by the *post hoc* insertion of empirical energy levels, something that is explicitly allowed for in the ExoMol data format (Tennyson et al. 2013). The HCN line list both in its original and updated forms has proved to be highly useful and indeed underpins a number of recent (possible) detections of HCN in exoplanets (Tsiaras et al. 2016; Hawker et al. 2018; Gandhi et al. 2020) and much exoplanet modelling; it has also been found useful for combustion studies (Glarborg & Marshall 2017). We would anticipate the OYT3 SiO₂ line list being used in a similar fashion and, should high resolution SiO₂ spectra become available, we will update the line list to improve its accuracy. However, we are unaware of any such studies in progress at present.

For present use, we recommend the OYT3 line list for low-resolution studies of exoplanet atmospheres, e.g. with a resolving power of $R \approx 100$, but we emphasise that the line list is not designed for high-resolution analysis. Interestingly, a recent cold molecular beam study has shown that silicon dioxide can be efficiently formed through the reaction of SiH and O₂ under single collision conditions (Yang et al. 2018), demonstrating a low-temperature pathway to gas-phase SiO₂ that is plausible in the interstellar medium or molecular clouds. The OYT3 line list will aid other astronomical searches for SiO₂ and may find use in industrial processes, for example, in the semiconductor industry where silicon-bearing molecules are commonly encountered.

ACKNOWLEDGMENTS

This work was supported by the STFC Projects No. ST/M001334/1 and ST/R000476/1. The authors acknowledge the use of the UCL Legion High Performance Computing Facility (Legion@UCL) and associated support services in the completion of this work, along with the Cambridge Service for Data Driven Discovery (CSD3), part of which is operated by the University of Cambridge Research Computing on behalf of the STFC DiRAC HPC Facility (www.dirac.ac.uk). The DiRAC component of CSD3 was funded by BEIS capital funding via STFC capital grants ST/P002307/1 and ST/R002452/1 and STFC operations grant ST/R00689X/1. DiRAC is part of the National e-Infrastructure.

REFERENCES

- Adler T. B., Knizia G., Werner H. J., 2007, *J. Chem. Phys.*, 127, 221106
 Amaral P. H. R., Diniz L. G., Jones K. A., Stanke M., Alijah A., Adamowicz L., Mohallem J. R., 2019, *ApJ*, 878, 95
 Andrews L., McCluskey M., 1992, *J. Mol. Spectrosc.*, 154, 223
 Barber R. J., Strange J. K., Hill C., Polyansky O. L., Mellau G. C., Yurchenko S. N., Tennyson J., 2014, *MNRAS*, 437, 1828
 Barton E. J., Yurchenko S. N., Tennyson J., 2013, *MNRAS*, 434, 1469
 Brinkmann N. R., Tschumper G. S., Schaefer III H. F., 1999, *J. Chem. Phys.*, 110, 6240
 Brown J. M. et al., 1975, *J. Mol. Spectrosc.*, 55, 500
 Bunker P. R., Jensen P., 1998, *Molecular Symmetry and Spectroscopy*, 2nd edn. NRC Research Press, Ottawa
 Carter S., Handy N., Sutcliffe B., 1983, *Mol. Phys.*, 49, 745
 CFOUR, 2019. A quantum chemical program package written by J. F. Stanton, J. Gauss, M. E. Harding, and P. G. Szalay with contributions from A. A. Auer, R. J. Bartlett, U. Benedikt, C. Berger, D. E. Bernholdt, Y. J. Bomble, L. Cheng, O. Christiansen,

- M. Heckert, O. Heun, C. Huber, T.-C. Jagau, D. Jonsson, J. Jusélius, K. Klein, W. J. Lauderdale, D. A. Matthews, T. Metzroth, L. A. Mück, D. P. O'Neill, D. R. Price, E. Prochnow, C. Puzzarini, K. Ruud, F. Schiffrmann, W. Schwalbach, S. Stopkowicz, A. Tajti, J. Vázquez, F. Wang, J. D. Watts, and the integral packages MOLECULE (J. Almlöf and P. R. Taylor), PROPS (P. R. Taylor), ABACUS (T. Helgaker, H. J. Aa. Jensen, P. Jørgensen, and J. Olsen), and ECP routines by A. V. Mitin and C. van Wüllen. For the current version, see <http://www.cfour.de>.
- Chubb K. L., Yachmenev A., Tennyson J., Yurchenko S. N., 2018, *J. Chem. Phys.*, 149, 014101
- Clark V. H. J., Owens A., Tennyson J., Yurchenko S. N., 2020, *J. Quant. Spectrosc. Radiat. Transf.*, 246, 106929
- Cooley J. W., 1961, *Math. Comp.*, 15, 363
- Coppola C. M., Lodi L., Tennyson J., 2011, *MNRAS*, 415, 487
- Császár A. G., Allen W. D., Schaefer III H. F., 1998, *J. Chem. Phys.*, 108, 9751
- de Jong W. A., Harrison R. J., Dixon D. A., 2001, *J. Chem. Phys.*, 114, 48
- Demory B.-O. et al., 2016, *Nature*, 532, 207
- Douglas M., Kroll N. M., 1974, *Ann. Phys.*, 82, 89
- Dunning T. H., 1989, *J. Chem. Phys.*, 90, 1007
- Engel E. A., Doss N., Harris G. J., Tennyson J., 2005, *MNRAS*, 357, 471
- Fegley, Jr. B., Jacobson N. S., Williams K. B., Plane J. M. C., Schaefer L., Lodders K., 2016, *ApJ*, 824, 103
- Gandhi S. et al., 2020, *MNRAS*
- Glarborg P., Marshall P., 2017, *Energy & Fuels*, 31, 2156
- Gorman M., Yurchenko S. N., Tennyson J., 2019, *MNRAS*, 490, 1652
- Hao Y., Xie Y., Schaefer III H. F., 2014, *RSC Adv.*, 4, 47163
- Harris G. J., Larner F. C., Tennyson J., Kaminsky B. M., Pavlenko Y. V., Jones H. R. A., 2008, *MNRAS*, 390, 143
- Harris G. J., Polyansky O. L., Tennyson J., 2002, *ApJ*, 578, 657
- Harris G. J., Tennyson J., Kaminsky B. M., Pavlenko Y. V., Jones H. R. A., 2006, *MNRAS*, 367, 400
- Hättig C., 2005, *Phys. Chem. Chem. Phys.*, 7, 59
- Hawker G. A., Madhusudhan N., Cabot S. H. C., Gandhi S., 2018, *ApJL*, 863, L11
- Heß B. A., 1986, *Phys. Rev. A*, 33, 3742
- Hill J. G., Mazumder S., Peterson K. A., 2010, *J. Chem. Phys.*, 132, 054108
- Hill J. G., Peterson K. A., Knizia G., Werner H.-J., 2009, *J. Chem. Phys.*, 131, 194105
- Jacox M. E., 1994, *Chem. Phys.*, 189, 149
- Jørgensen U. G., Jensen P., 1993, *J. Mol. Spectrosc.*, 161, 219
- Kállay M., Gauss J., 2005, *J. Chem. Phys.*, 123, 214105
- Kállay M., Gauss J., 2008, *J. Chem. Phys.*, 129, 144101
- Kaufman M., Muentner J., Klemperer W., 1967, *J. Chem. Phys.*, 47, 3365
- Kostko O., Ahmed M., Metz R. B., 2009, *J. Phys. Chem. A*, 113, 1225
- Miguel Y., Kaltenecker L., Fegley B., Schaefer L., 2011, *ApJ*, 742, L19
- Mizus I. I., Alijah A., Zobov N. F., Kyuberis A. A., Yurchenko S. N., Tennyson J., Polyansky O. L., 2017, *MNRAS*, 468, 1717
- MRCC, 2019. A string-based quantum chemical program suite written by M. Kállay, See also M. Kállay and P. R. Surján, *J. Chem. Phys.* **115**, 2945 (2001) as well as www.mrcc.hu.
- Neale L., Miller S., Tennyson J., 1996, *ApJ*, 464, 516
- Noumerov B. V., 1924, *MNRAS*, 84, 592
- Owens A., Yachmenev A., Küpper J., Yurchenko S. N., Thiel W., 2018, *Phys. Chem. Chem. Phys.*, 21, 3496
- Owens A., Yurchenko S. N., 2019, *J. Chem. Phys.*, 150, 194308
- Owens A., Yurchenko S. N., Yachmenev A., Tennyson J., Thiel W., 2015a, *J. Chem. Phys.*, 142, 244306
- Owens A., Yurchenko S. N., Yachmenev A., Tennyson J., Thiel W., 2016, *J. Chem. Phys.*, 145, 104305
- Owens A., Yurchenko S. N., Yachmenev A., Thiel W., 2015b, *J. Chem. Phys.*, 143, 244317
- Owens A., Yurchenko S. N., Yachmenev A., Thiel W., Tennyson J., 2017, *MNRAS*, 471, 5025
- Pacansky J., Hermann K., 1978, *J. Chem. Phys.*, 69, 963
- Partridge H., Schwenke D. W., 1997, *J. Chem. Phys.*, 106, 4618
- Peterson K. A., Adler T. B., Werner H.-J., 2008, *J. Chem. Phys.*, 128, 084102
- Polyansky O. L., Kyuberis A. A., Zobov N. F., Tennyson J., Yurchenko S. N., Lodi L., 2018, *MNRAS*, 480, 2597
- Schaefer L., Fegley B., 2009, *ApJ*, 703, L113
- Schaefer L., Lodders K., Fegley, Jr. B., 2012, *ApJ*, 755, 41
- Schnöckel H., 1978, *Angew. Chem. Int. Ed. Engl.*, 17, 616
- Schnöckel H., 1980, *Z. anorg. allg. Chem.*, 460, 37
- Sutcliffe B. T., Tennyson J., 1991, *Int. J. Quantum Chem.*, 39, 183
- Ten-No S., 2004, *Chem. Phys. Lett.*, 398, 56
- Tennyson J., 2012, *WIREs Comput. Mol. Sci.*, 2, 698
- Tennyson J., 2014, *J. Mol. Spectrosc.*, 298, 1
- Tennyson J., 2016, *J. Chem. Phys.*, 145, 120901
- Tennyson J., Hill C., Yurchenko S. N., 2013, in *AIP Conference Proceedings*, Vol. 1545, 6th international conference on atomic and molecular data and their applications ICAMDATA-2012, AIP, New York, pp. 186–195
- Tennyson J., Kostin M. A., Barletta P., Harris G. J., Polyansky O. L., Ramanlal J., Zobov N. F., 2004, *Comput. Phys. Commun.*, 163, 85
- Tennyson J., Sutcliffe B. T., 1982, *J. Chem. Phys.*, 77, 4061
- Tennyson J., Sutcliffe B. T., 1986, *Mol. Phys.*, 58, 1067
- Tennyson J., Sutcliffe B. T., 1992, *Int. J. Quantum Chem.*, 42, 941
- Tennyson J., Yurchenko S. N., 2012, *MNRAS*, 425, 21
- Tennyson J., Yurchenko S. N., 2017a, *Mol. Astrophys.*, 8, 1

- Tennyson J., Yurchenko S. N., 2017b, *Int. J. Quantum Chem.*, 117, 92
 Tennyson J., Yurchenko S. N., 2018, *Atoms*, 6, 26
 Tennyson J. et al., 2016, *J. Mol. Spectrosc.*, 327, 73
 Tsiaras A. et al., 2016, *ApJ*, 820, 99
 Tyuterev V. G., Tashkun S. A., Schwenke D. W., 2001, *Chem. Phys. Lett.*, 348, 223
 Upadhyay A., Conway E. K., Tennyson J., Yurchenko S. N., 2018, *MNRAS*, 477, 1520
 van Mourik T., Harris G. J., Polyansky O. L., Tennyson J., Császár A. G., Knowles P. J., 2001, *J. Chem. Phys.*, 115, 3706
 Wang L.-S., Wu H., Desai S. R., Fan J., Colson S. D., 1996, *J. Phys. Chem.*, 100, 8697
 Watson J. K. G., 2003, *J. Mol. Spectrosc.*, 219, 326
 Weck P. F., Stancil P. C., Kirby K., 2003, *J. Chem. Phys.*, 118, 9997
 Weigend F., 2002, *Phys. Chem. Chem. Phys.*, 4, 4285
 Werner H.-J., Knowles P. J., Knizia G., Manby F. R., Schütz M., 2012, *WIREs Comput. Mol. Sci.*, 2, 242
 Yachmenev A., Yurchenko S. N., 2015, *J. Chem. Phys.*, 143, 014105
 Yachmenev A., Yurchenko S. N., Ribeyre T., Thiel W., 2011, *J. Chem. Phys.*, 135, 074302
 Yang T., Thomas A. M., Dangi B. B., Kaiser R. I., Mebel A. M., Millar T. J., 2018, *Nat. Commun.*, 9
 Yousaf K. E., Peterson K. A., 2008, *J. Chem. Phys.*, 129, 184108
 Yurchenko S. N., 2014, in *Chemical Modelling: Volume 10*, Vol. 10, The Royal Society of Chemistry, pp. 183–228
 Yurchenko S. N., Al-Refaie A. F., Tennyson J., 2018, *A&A*, 614, A131
 Yurchenko S. N., Barber R. J., Yachmenev A., Thiel W., Jensen P., Tennyson J., 2009, *J. Phys. Chem. A*, 113, 11845
 Yurchenko S. N., Tennyson J., Miller S., Melnikov V. V., O'Donoghue J., Moore L., 2020, *MNRAS*
 Yurchenko S. N., Thiel W., Jensen P., 2007, *J. Mol. Spectrosc.*, 245, 126
 Yurchenko S. N., Yachmenev A., Ovsyannikov R. I., 2017, *J. Chem. Theory Comput.*, 13, 4368

SUPPORTING INFORMATION

Supplementary data are available at MNRAS online. This includes the potential energy and dipole moment surfaces of SiO₂ with programs to construct them, and values of the temperature-dependent partition function of SiO₂ up to 3000 K. The following references were cited in the supplementary material: (Owens et al. 2015a,b, 2016, 2018; Owens & Yurchenko 2019; Császár et al. 1998; Adler et al. 2007; Peterson et al. 2008; Hill et al. 2009; Ten-No 2004; Yousaf & Peterson 2008; Weigend 2002; Hättig 2005; Werner et al. 2012; Yachmenev et al. 2011; Hill et al. 2010; Kállay & Gauss 2005, 2008; MRCC 2019; CFOUR 2019; Dunning 1989; Douglas & Kroll 1974; Heß 1986; de Jong et al. 2001; Tyuterev et al. 2001; Partridge & Schwenke 1997; Watson 2003; Jørgensen & Jensen 1993; Yurchenko et al. 2007, 2009; Yachmenev & Yurchenko 2015; Tennyson & Yurchenko 2017b; Yurchenko et al. 2017; Chubb et al. 2018; Carter et al. 1983; Sutcliffe & Tennyson 1991; Noumerov 1924; Cooley 1961; Tennyson & Sutcliffe 1986; Tennyson et al. 2004; Tennyson & Sutcliffe 1992, 1982; Yurchenko et al. 2018)